Progress In Electromagnetics Research, PIER 36, 319–335, 2002

MODE-MATCHING ANALYSIS OF WAVEGUIDE T-JUNCTION LOADED WITH AN H-PLANE DIELECTRIC SLAB

Z. Jiang, Z. Shen, and X. Shan

School of Electrical and Electronic Engineering
Nanyang Technological University
Nanyang Avenue, Singapore 639798

Abstract—This paper presents a full-wave mode-matching analysis of a rectangular waveguide T-junction partially loaded with an H-plane dielectric slab. First, the longitudinal section electric (LSE) and longitudinal section magnetic (LSM) modes in an H-plane dielectric-filled rectangular waveguide are obtained. Second, the dielectric-loaded T-junction is then divided into four regions and their electromagnetic fields are expanded into the summation of their modal functions using the resonator method. Finally, a mode-matching process for the tangential field components across regional interfaces is carried out to derive the generalized scattering matrix of the waveguide T-junction. Using the cascading connection technique of generalized scattering matrix, various waveguide couplers and power dividers/combiners with H-plane dielectric slabs can be easily analyzed and designed. Numerical results are presented and compared with those obtained by measurement or Ansoft's HFSS. Good agreement is observed.

1. INTRODUCTION

Rectangular waveguide T-junction is a basic passive microwave component and it has found wide applications in waveguide directional couplers [1–4], power dividers/combiners [5, 6], filters [7] and multiplexers [8] for modern radar and satellite communication systems.

Compared to the conventional air-filled waveguide T-junction, using dielectric filling can obviously reduce the size of the T-junction and in turn reduce the dimensions of various waveguide passive components, i.e., couplers, power dividers/combiners. Employing dielectric loading can also provide some other useful characteristics compared to the standard air-filled waveguide T-junction. For example, the power carried along a dielectric-filled waveguide is confined primarily to the interior of the dielectric slab. This can reduce the radiation loss and facilitate a tight coupling from the main waveguide to the side arm of a waveguide T-junction when a dielectric slab is inserted into the part close to the side arm.

The standard air-filled rectangular waveguide T-junction has been extensively investigated by a number of researchers [6–13]. Although the structure is potentially very useful, it appears that no study of the problem of a rectangular waveguide T-junction loaded with an H-plane dielectric slab has been reported in the literature, to the authors' best knowledge.

This paper presents a rigorous analysis of a rectangular waveguide T-junction having an H-plane dielectric slab partially filled in the main waveguide using the mode-matching method. The electromagnetic fields in the T-junction are expanded into the summation of a series of eigen modes and the derived generalized scattering matrix of the waveguide T-junction can be directly used in the synthesis of various waveguide components. Compared to other numerical techniques, the mode-matching method is formally exact and has been proved to be very efficient. The cross-section of the side-arm waveguide in the T-junction can also be arbitrary and the two coupling waveguides can be dissimilar [14].

This paper is organized as follows. In Section 2, we first describe the modes in a dielectric-filled waveguide. Then, the derivation of the generalized scattering matrix is presented for an H-plane dielectric-filled rectangular waveguide T-junction with an arbitrary side arm. The scattering matrices of various single-aperture coupling structures such as waveguide couplers or power dividers/combiners can be obtained directly by cascading two three-port T-junctions together. Cascading a number of single-aperture coupling elements together can also provide the scattering matrix of a multi-aperture coupling

structure. In Section 3, we first verify the scattering parameter results for two rectangular waveguide T-junctions with and without dielectric slab insertion, respectively. Then, three examples of dielectric-filled waveguide couplers and power divider/combiner designed at X-band using rectangular apertures are presented. The calculated scattering parameters by our mode-matching method are compared with the available measured or simulated results by Ansoft's HFSS. Excellent agreement has been observed for all the cases considered.

2. FORMULATION

This section presents the theoretical formulation for the generalized scattering matrix of an H-plane dielectric-slab-loaded waveguide T-junction. First, we give the LSE and LSM modes in an H-plane dielectric-filled rectangular waveguide. Then. The mode matching method is used to derive the generalized scattering matrix of the dielectric-filled waveguide T-junction.

2.1. Modes in a Dielectric-filled Waveguide

Figure 1 illustrates the cross-section of an H-plane dielectric-filled rectangular waveguide.

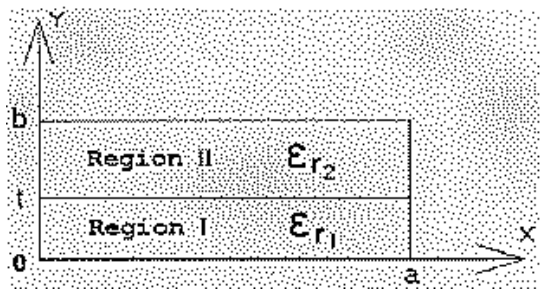

Figure 1. Cross-section of an H-plane dielectric-filled waveguide.

It is known that the normal modes of propagation for a waveguide loaded with dielectric slabs, as shown in Fig. 1, are not, in general, either **E** or **H** modes, but combinations of an **E** and an **H** mode. As the boundary conditions at the interface ($y = t$) can be satisfied by **E** or **H** modes alone at xz-plane, we know that the basic modes of propagation for slab-loaded rectangular guides may be derived from magnetic and electric types of Hertzian potential functions, having single components directed normal to the interface of two dielectric layers [15, 16]. The derived modes are called longitudinal section

electric (LSE) and longitudinal section magnetic (LSM) modes, which can be written in the following forms.

$$\text{LSE modes:} \quad \Psi_h = \begin{cases} A_h \cos\dfrac{n\pi x}{a}\sin(k_{y1}y) & 0 \le y \le t \\ B_h \cos\dfrac{n\pi x}{a}\sin[k_{y2}(b-y)] & t \le y \le b \end{cases} \tag{1}$$

$$\text{LSM modes:} \quad \Psi_e = \begin{cases} A_e \sin\dfrac{n\pi x}{a}\cos(k_{y1}y) & 0 \le y \le t \\ B_e \sin\dfrac{n\pi x}{a}\cos[k_{y2}(b-y)] & t \le y \le b \end{cases} \tag{2}$$

where $\Psi_{(h,e)}$ are the potential functions for LSE and LSM modes, respectively. $A_{(e,h)}$ and $B_{(e,h)}$ are the modal amplitude coefficients, which can be related to each other during the mode-matching process. k_{y1} and k_{y2} can be derived from

$$k_{y1}^2 = k^2\varepsilon_{r1} + \gamma^2 - \left(\frac{n\pi}{a}\right)^2 \tag{3a}$$

$$k_{y2}^2 = k^2\varepsilon_{r2} + \gamma^2 - \left(\frac{n\pi}{a}\right)^2 \tag{3b}$$

where γ is the propagation constant of the LSE or LSM mode. ε_{r1} and ε_{r2} are the relative permittivities for Region I and Region II, respectively. k is the wavenumber in the free space. The electromagnetic fields in Fig. 1 can be obtained from

$$\text{LSE modes:} \quad \begin{cases} \vec{E} = -j\omega\mu_0\nabla\times\vec{\Pi}_h \\ \vec{H} = \nabla\times\nabla\times\vec{\Pi}_h \end{cases} \tag{4}$$

$$\text{LSM modes:} \quad \begin{cases} \vec{E} = \nabla\times\nabla\times\vec{\Pi}_e \\ \vec{H} = j\omega\varepsilon_{(1,2)}\nabla\times\vec{\Pi}_e \end{cases} \tag{5}$$

where the magnetic-type Hertzian potential for LSE modes is $\vec{\Pi}_h = \hat{a}_y\Psi_h(x,y)e^{-\gamma z}$ and the electric-type Hertzian potential for LSM modes is $\vec{\Pi}_e = \hat{a}_y\Psi_e(x,y)e^{-\gamma z}$ with the assumption that z is the propagation direction.

2.2. Waveguide T-junction

Figure 2 illustrates the waveguide T-junction partially loaded with an H-plane dielectric slab. The cross-section of the side arm can be arbitrary.

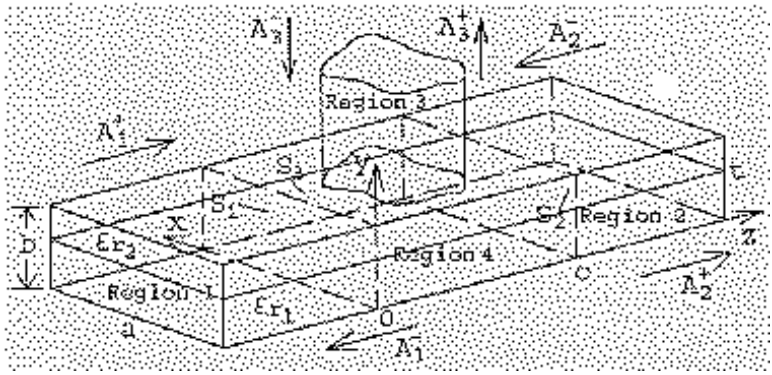

Figure 2. Waveguide T-junction partially loaded with an H-plane dielectric slab.

The whole waveguide T-junction is divided into four regions: 1, 2, 3, and 4. Regions 1 and 2 are dielectric-filled semi-infinite rectangular waveguides, where the expansion expressions of the electromagnetic fields can be easily obtained from subsection 2.1. Region 3 is a homogeneous semi-infinite waveguide of arbitrary cross-section, whose modal functions and cutoff wavenumbers are available. Interface S_1 is at $z = 0$, S_2 at $z = c$, and S_3 is at $y = b$ $(0 < x < a,\ 0 < z < c)$.

The electromagnetic fields in the above three semi-infinite waveguides can be expressed as [6]:

$$\vec{E}^{(v)} = \frac{1}{j\omega\varepsilon}\nabla \times \nabla \times \vec{A}_e^{(v)} + \nabla \times \vec{A}_h^{(v)} \tag{6a}$$

$$\vec{H}^{(v)} = \frac{1}{-j\omega\mu}\nabla \times \nabla \times \vec{A}_h^{(v)} + \nabla \times \vec{A}_e^{(v)} \tag{6b}$$

where $v = 1, 2, 3$, $\vec{A}_h$ and $\vec{A}_e$ are the vector potentials for LSE, LSM modes $(v = 1, 2)$ or TE, TM modes $(v = 3)$, respectively. For Regions 1 and 2, we can have the following forms for $\vec{A}_h^{(1,2)}$ and $\vec{A}_e^{(1,2)}$:

$$\begin{aligned}
\vec{A}_h^{(1,2)} &= \vec{a}_z \sum_{i=1}^{N_h} N_{hi}^{(1,2)} \Psi_{hi}^{(1,2)} [A_{1,2hi}^{+} e^{-\gamma_{1,2hi} z} + A_{1,2hi}^{-} e^{+\gamma_{1,2hi} z}] \\
\vec{A}_e^{(1,2)} &= \vec{a}_z \sum_{i=1}^{N_e} N_{ei}^{(1,2)} \Psi_{ei}^{(1,2)} [A_{1,2ei}^{+} e^{-\gamma_{1,2ei} z} - A_{1,2ei}^{-} e^{+\gamma_{1,2ei} z}]
\end{aligned} \tag{7}$$

where A_{1i}^{+} and A_{1i}^{-} are the modal amplitude coefficients of the incident $(+)$ and reflected $(-)$ waves in waveguide Region 1; A_{2i}^{-} and A_{2i}^{+} are

the modal amplitude coefficients of the incident (−) and reflected (+) modes in waveguide Region 2.

For Region 3, we can have the following forms for $\vec{A}_h^{(3)}$ and $\vec{A}_e^{(3)}$:

$$\begin{aligned}\vec{A}_h^{(3)} &= \vec{a}_y \sum_{j=1}^{M_h} N_{hj}^{(3)} \Psi_{hj}^{(3)} [A_{3hj}^{+} e^{-\gamma_{3hj} y} + A_{3hj}^{-} e^{+\gamma_{3hj} y}] \\ \vec{A}_e^{(3)} &= \vec{a}_y \sum_{j=1}^{M_e} N_{ej}^{(3)} \Psi_{ej}^{(3)} [A_{3ej}^{+} e^{-\gamma_{3ej} y} - A_{3ej}^{-} e^{+\gamma_{3ej} y}]\end{aligned} \tag{8}$$

where A_{3j}^{+}, A_{3j}^{-} are the modal amplitude coefficients of the reflected (+) and incident (−) waves in the side arm; γ_h and γ_e are the propagation constants of the TE and TM modes, respectively; i and j are the mode indexes; $N_{(he)}^{(v)}$ are the normalized factors such that the power carried by each mode is 1 W. $\Psi_{(h,e)}^{(v)}$ is the modal function for different regions. For Regions 1 and 2, the modal functions $\Psi_{(h,e)}^{(1,2)}$ are given in subsection 2.1. For Region 3, the modal functions $\Psi_h^{(3)}$ and $\Psi_e^{(3)}$ will depend on the waveguide cross section of the side arm considered.

For Region 4, the resonator method [17, 18] is employed to obtain its electromagnetic fields by superimposing three suitably chosen standing-wave solutions:

$$A_{h,e}^{(4)} = A_{h,e}^{(4)(1)} + A_{h,e}^{(4)(2)} + A_{h,e}^{(4)(3)} \tag{9}$$

where solution $A_{h,e}^{(4)(1)}$ is obtained when the boundary planes S_2 and S_3 in Fig. 2 are short-circuited and S_1 is left open; solutions $A_{h,e}^{(4)(2)}$ and $A_{h,e}^{(4)(3)}$ are obtained in a similar way.

Once all the field expressions for all the four regions are available, we then match the tangential electric and magnetic fields along the three regional interfaces S_1, S_2, and S_3. The relationship between the modal amplitude coefficients ($A_{(v)}^{+}$ and $A_{(v)}^{-}$, $v = 1, 2, 3$) of the three semi-infinite waveguides can be derived to result in the desired generalized scattering matrix of the waveguide T-junction. For the rectangular waveguide T-junction having a side arm of arbitrary shape, as shown in Fig. 2, the final scattering matrix can be written as:

$$[\mathbf{S_{T-junction}}] = \begin{bmatrix} \mathbf{S_{11}} & \mathbf{S_{12}} & \mathbf{S_{13}} \\ \mathbf{S_{21}} & \mathbf{S_{22}} & \mathbf{S_{23}} \\ \mathbf{S_{31}} & \mathbf{S_{32}} & \mathbf{S_{33}} \end{bmatrix} = \begin{bmatrix} \mathbf{A} & \mathbf{B} & \mathbf{C} \\ \mathbf{B} & \mathbf{A} & \mathbf{D} \\ \mathbf{E} & \mathbf{F} & \mathbf{G} \end{bmatrix}^{-1} - \mathbf{I} \tag{10}$$

where

$$\mathbf{C} = \frac{\mathbf{1}}{\mathbf{2}}\mathbf{H_1 M_A} \tag{11}$$

$$\mathbf{D} = -\frac{\mathbf{1}}{\mathbf{2}}\mathbf{H_2 M_A} \tag{12}$$

$$\mathbf{G} = \frac{\mathbf{1}}{\mathbf{2}}(\mathbf{I} - \mathbf{Y_3^{-1}} \mathbf{M_A^T Y_{4,II} G_P M_A}) \tag{13}$$

$$\mathbf{E} = -\frac{\mathbf{1}}{\mathbf{2}}(\mathbf{W_A} - \mathbf{W_B L_1^2})(\mathbf{I} - \mathbf{L_1^2})^{\mathbf{-1}} \tag{14}$$

$$\mathbf{F} = \frac{\mathbf{1}}{\mathbf{2}}(\mathbf{W_A} - \mathbf{W_B})\mathbf{L_1}(\mathbf{I} - \mathbf{L_1^2})^{\mathbf{-1}} \tag{15}$$

with

$$A_{i,j} = \frac{1}{1 - e^{-2\gamma_{1i}C}}\delta_{i,j} \tag{16}$$

$$B_{i,j} = \frac{e^{-\gamma_{1i}C}}{e^{-2\gamma_{1i}C} - 1}\delta_{i,j} \tag{17}$$

$$L_{1i,j} = e^{-\gamma_{1i}C}\delta_{i,j} \tag{18}$$

$$\begin{aligned} H_{1,ik} = {} & \int_{S_{1,I}} \vec{e}_{1it,I} \times \frac{2e^{-\gamma_{4k,II}(t-b)}}{P_1 G_S} \{[-\cosh(\gamma_{4k,I} y)]\, h_{x4k,I}\hat{x} \\ & + [\sinh(\gamma_{4k,I} y)]\, h_{y4k,I}\hat{y}\} \cdot \vec{ds} + \int_{S_{1,II}} \vec{e}_{1it,II} \\ & \times \left\{ \left[e^{-\gamma_{4k,II}(y-b)} - \frac{Q_1 e^{-2\gamma_{4k,II}}(t-b)}{P_1} e^{\gamma_{4k,II}(y-b)} \right] h_{x4k,II}\hat{x} \right. \\ & \left. + \left[e^{-\gamma_{4k,II}(y-b)} + \frac{Q_1 e^{-2\gamma_{4k,II}(t-b)}}{P_1} e^{\gamma_{4k,II}(y-b)} \right] h_{y4k,II}\hat{y} \right\} \cdot \frac{\vec{ds}}{G_S} \end{aligned} \tag{19}$$

$$M_{A,kj} = \int_{S_3} (\vec{e}_{4kt} \cdot \vec{e}_{3jt}) ds = \int_{S_3} (\hat{y} \times \vec{e}_{4kt}) \cdot (\hat{y} \times \vec{e}_{3jt}) ds \tag{20}$$

$$H_{2,ik} = (-1)^{n^{(4)}+1} H_{1,ik} \tag{21}$$

$$W_{A,ji} = \frac{1}{Y_{3j}} \int_{S_3} \hat{y} \times \vec{e}_{3jt} \cdot e^{-\gamma_{1i}z} [h_{z1i,II}\hat{z} + h_{x1i,II}\hat{x}] \Big|_{y=b_2} ds \tag{22}$$

$$W_{B,ji} = \frac{1}{Y_{3j}} \int_{S_3} \hat{y} \times \vec{e}_{3jt} \cdot e^{\gamma_{1i}z} [h_{z1i,II}\hat{z} - h_{x1i,II}\hat{x}] \Big|_{y=b_2} ds \tag{23}$$

and

$$P_{1,k} = \sinh(\gamma_{4k,I} t) - \cosh(\gamma_{4k,I} t) \frac{Y_{4k,I}}{Y_{4k,II}} \tag{24}$$

$$Q_{1,k} = \sinh(\gamma_{4k,I}t) + \cosh(\gamma_{4k,I}t)\frac{Y_{4k,I}}{Y_{4k,II}} \tag{25}$$

$$G_{S,k} = 1 + \frac{e^{-2\gamma_{4k,II}(t-b)}Q_{1,k}}{P_{1,k}} \tag{26}$$

$$G_{p,k} = \frac{1 - \dfrac{e^{-2\gamma_{4k,II}(t-b)}Q_{1,k}}{P_{1,k}}}{1 + \dfrac{e^{-2\gamma_{4k,II}(t-b)}Q_{1,k}}{P_{1,k}}} \tag{27}$$

$$h_{x4k(I,II)} = \begin{cases} \dfrac{\sqrt{\left(\frac{l^{(4)}\pi}{a}\right)^2 + \left(\frac{n^{(4)}\pi}{c}\right)^2 - k^2\varepsilon_{r1,2}}}{j\omega\mu} \cdot \left(\dfrac{l^{(4)}\pi}{a}\right) \\ \quad \cdot N_{ln}^{(4)} \cdot \sin\dfrac{l^{(4)}\pi x}{a}\cos\dfrac{n^{(4)}\pi z}{c} & \text{TE-modes} \\ \dfrac{j\omega\varepsilon_{r1,2}}{\sqrt{\left(\frac{l^{(4)}\pi}{a}\right)^2 + \left(\frac{n^{(4)}\pi}{c}\right)^2 - k^2\varepsilon_{r1,2}}} \cdot \left(\dfrac{n^{(4)}\pi}{a}\right) \\ \quad \cdot N_{ln}^{(4)} \cdot \sin\dfrac{l^{(4)}\pi x}{a}\cos\dfrac{n^{(4)}\pi z}{c} & \text{TM-modes} \end{cases} \tag{28}$$

$$h_{y4k(I,II)} = \begin{cases} \dfrac{\left(\frac{l^{(4)}\pi}{a}\right)^2 + \left(\frac{n^{(4)}\pi}{c}\right)^2}{j\omega\mu} \cdot N_{ln}^{(4)} \\ \quad \cdot \cos\dfrac{l^{(4)}\pi x}{a}\cos\dfrac{n^{(4)}\pi z}{c} & \text{TE-modes} \\ 0 & \text{TM-modes} \end{cases} \tag{29}$$

$$h_{z1i,II} = \begin{cases} (-\gamma_{1i}k_{y2})\dfrac{\sin(k_{y1}t)}{\sin(k_{y2}(b-t))} \\ \quad \cdot \cos(k_{y2}(b-y)) \cdot \cos\frac{n^{(1)}\pi x}{a} \cdot N_{LSE} & \text{LSE-modes} \\ (-j\omega\varepsilon_{r1})\left(\dfrac{n^{(1)}\pi}{a}\right)\dfrac{\cos(k_{y1}t)}{\cos(k_{y2}(b-t))} \\ \quad \cdot \cos(k_{y2}(b-y)) \cdot \cos\frac{n^{(1)}\pi x}{a} \cdot N_{LSM} & \text{LSM-modes} \end{cases} \tag{30}$$

$$h_{x1i,II} = \begin{cases} \left(-\dfrac{n^{(1)}\pi}{a}\cdot k_{y2}\right)\dfrac{\sin(k_{y1}t)}{\sin(k_{y2}(b-t))} \\ \quad \cdot\cos(k_{y2}(b-y))\cdot\sin\dfrac{n^{(1)}\pi x}{a}\cdot N_{LSE} & \text{LSE-modes} \\ (-j\omega\varepsilon_{r1})\gamma_{1i}\dfrac{\cos(k_{y1}t)}{\cos(k_{y2}(b-t))} \\ \quad \cdot\cos(k_{y2}(b-y))\cdot\sin\dfrac{n^{(1)}\pi x}{a}\cdot N_{LSM} & \text{LSM-modes} \end{cases} \tag{31}$$

In (13), $\mathbf{Y}_3$ is the diagonal admittance matrix for the side arm waveguide, which is defined as $Y_{3i} = \gamma_{3i}/j\omega\mu$ for **TE** modes and $Y_{3i} = j\omega\varepsilon/\gamma_{3i}$ for **TM** modes. $\mathbf{Y}_{4(I,II)}$ are the admittance matrices for Region 4(I) and Region 4(II), respectively. $\delta_{i,j}$ is the Kronecker delta, which is defined as $\delta_{i,j} = 0$ for $i \neq j$, and $\delta_{i,j} = 1$ for $i = j$. The matrix $\mathbf{M_A}$ the E-field mode-matching matrix at interface S_3 and the superscript "**T**" denotes the transpose operation. $\vec{e}_{3jt}$ is the normalized transverse component of the electric field for the j^{th} mode in the side arm, which has the form of:

$$\vec{e}_{3jt} = \begin{cases} \hat{y}\times\nabla_t N^h_{3j}\Psi^h_{3j} & \text{TE-modes} \\ \nabla_t N^e_{3j}\Psi^e_{3j} & \text{TM-modes} \end{cases} \tag{32}$$

$\vec{e}_{4kt}$ is the normalized transverse component of the electric field for the k^{th} mode in Region 4 and can be expressed using the same way as (32) in terms of its potential functions. $\vec{e}_{1it(I,II)}$ is the normalized transverse component of the electric field for the i^{th} mode in Region 1(I,II) and Region 2(I,II), which can be derived directly from the modal functions given in subsection 2.1.

It is noticed that equations (10)–(32) give a complete solution for the scattering parameters of an H-plane dielectric-slab-loaded rectangular waveguide T-junction having a side arm of arbitrary shape. For waveguide side arms of different shapes, the only difference will be in equations (20), (22), (23) due to the different $\vec{e}_{3jt}$ for different cross sections of the side arm.

The scattering parameters for a single-aperture coupler can be derived from the two scattering matrices of the basic T-junctions by cascading two three-port networks together. The diagonal transmission matrix of the side arm waveguide has its diagonal element of:

$$L_i = e^{-\gamma_{3i}\cdot t} = e^{-t\sqrt{k^2_{c,i}-k^2}} \tag{33}$$

with $k^2 = \omega^2\mu\varepsilon$ and t being the thickness of the aperture. The effects from higher-order mode interaction are automatically included in the calculation when full sets of TE and TM modes in the side-arm waveguide are employed in the analysis.

3. NUMERICAL RESULTS

In order to verify the validity of our mode-matching formulation, five examples are considered: an air-filled rectangular waveguide T-junction; an H-plane dielectric-filled waveguide T-junction; two couplers employing transverse and longitudinal rectangular apertures, respectively, between two parallel dielectric-filled rectangular waveguides; and a 3 dB power divider designed for X-band slot antenna arrays. The results obtained by our method are then compared with the available measured data or those obtained by Ansoft's HFSS. Excellent agreement is achieved for all the cases considered.

An air-filled rectangular waveguide T-junction with the side arm also being a rectangular waveguide has been analyzed by other authors [6, 9]. The example of a rectangular waveguide (WR-137: $a_2 = 34.85$ mm, $b_2 = 15.799$ mm) T-junction with a side rectangular waveguide of reduced size (WR-90: $a_1 = 22.86$ mm, $b_1 = 10.16$ mm) located at the center of the broad wall, as shown in Fig. 3, is considered here first for comparison. By setting the relative permittivities ε_{r1} and ε_{r2} (in Fig. 2) to 1 for both Region I and Region II, the dielectric-filled T-junction shown in Fig. 2 will reduce to the conventional air-filled waveguide T-junction. The scattering parameters obtained by our mode-matching method are compared to the measured data given in [9]. Good agreement between them is observed. Only $|\mathbf{S_{11}}|$ and $|\mathbf{S_{21}}|$ are given in Fig. 3 because $|\mathbf{S_{31}}|$ and $|\mathbf{S_{33}}|$ can be readily calculated from $|\mathbf{S_{11}}|$ and $|\mathbf{S_{21}}|$ based on the unitary property of a lossless network. In our computation, 50 modes are considered in the main waveguide, 20 modes are used in the side arm and 35 modes are retained in Region 4.

Another waveguide T-junction of the same dimensions partially filled with an H-plane dielectric slab in the main waveguide is illustrated in Fig. 4. It is noticed that the behavior around the cutoff frequency of the first mode in the side arm (about 6.56 GHz in Fig. 3) is greatly altered after inserting the dielectric slab. The loading dielectric slab reduces the resonant frequency from 6.56 GHz to 5.55 GHz, as we expected. The relative permittivity ε_{r2} for the dielectric slab used in Fig. 4 is 2.5 and the thickness of the dielectric slab is $(b-t) = 8.299$ mm. Our mode-matching results are compared to those obtained by Ansoft's HFSS. It is seen that the agreement between them is very good.

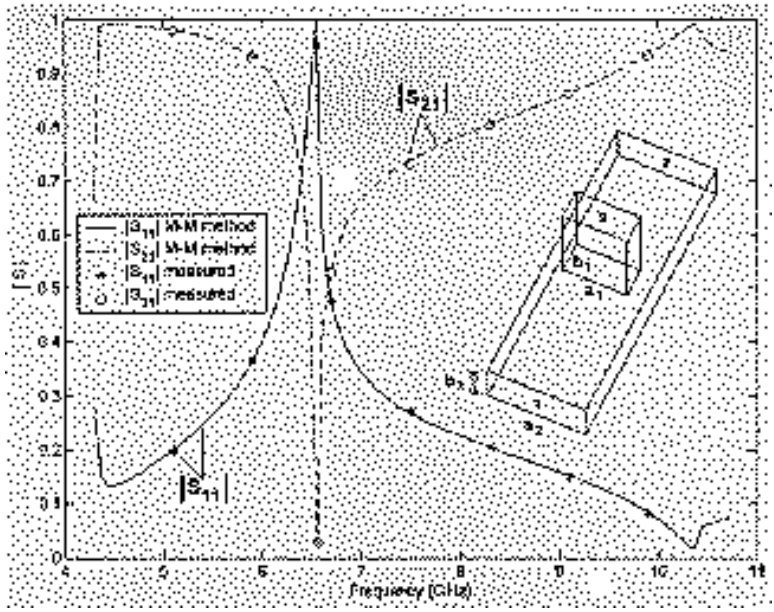

Figure 3. Scattering parameters of an air-filled rectangular waveguide T-junction with a side arm of reduced size waveguide ($a_2 = 34.85\,\text{mm}$, $b_2 = 15.799\,\text{mm}$, $a_1 = 22.86\,\text{mm}$, $b_1 = 10.16\,\text{mm}$).

By cascading two dielectric-filled waveguide T-junctions shown in Fig. 2, we can easily obtain a single-aperture waveguide coupler loaded with dielectric slabs, as shown in Fig. 5. It is clearly seen from Fig. 5 that the dimension of a waveguide coupler can be greatly reduced by inserting dielectric slabs. The relative permittivity ε_{r2} for the two identical dielectric slabs used in Fig. 5 is 3.5 and the thickness of the dielectric slabs is $(b - t) = 5.0\,\text{mm}$. The thickness of the aperture is $th = 1.0\,\text{mm}$. The aperture lies at the center of the broad walls of two identical dielectric-filled waveguides. 30 modes are employed in the analysis for the rectangular aperture. Comparing the calculated results using different ε_{r2}, it is easy to see that a tighter coupling through the aperture can be readily realized by employing a slab of larger ε_{r2}. The scattering parameters obtained by the mode-matching method are in good agreement with those calculated by Ansoft's HFSS.

A similar dielectric-filled rectangular waveguide coupler using longitudinal rectangular aperture is presented in Fig. 6. The off-center aperture is employed to facilitate a tight coupling. It is noticed that the same coupling can be realized with an aperture of reduced length by inserting the dielectric slabs in the main waveguides,

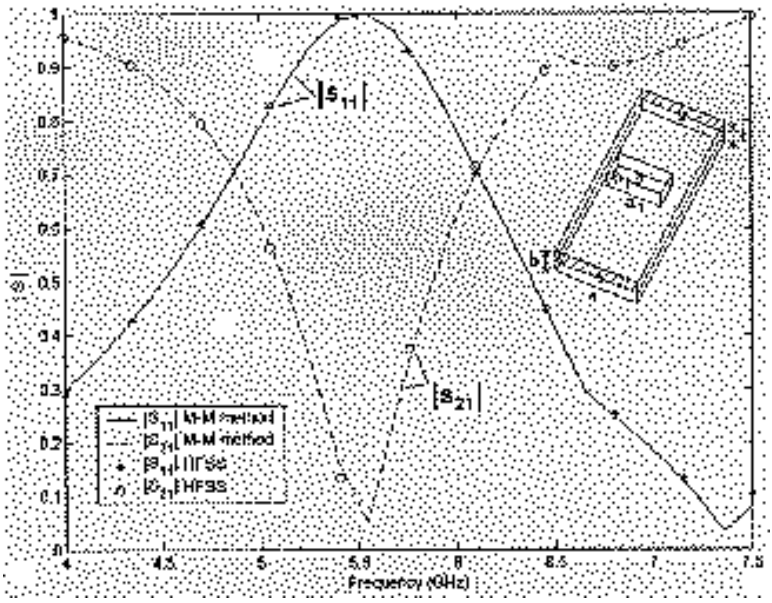

Figure 4. Scattering parameters of an H-plane dielectric-slab-loaded rectangular waveguide T-junction ($a = 34.85\,\text{mm}$, $b = 15.799\,\text{mm}$, $a_1 = 22.86\,\text{mm}$, $b_1 = 10.16\,\text{mm}$, $t = 7.5\,\text{mm}$, $\varepsilon_{r1} = 1$, $\varepsilon_{r2} = 2.5$).

compared to the conventional air-filled waveguides. The dimensions for the aperture used in Fig. 6 are: $a_1 = 5.0\,\text{mm}$, $b_1 = 9.4\,\text{mm}$ and thickness $th = 1.0\,\text{mm}$. The center-to-center offset for the aperture is $X_C = 4.5\,\text{mm}$. The relative permittivity ε_{r2} for two identical dielectric slabs used in Fig. 6 is 3.5 and the thickness of the dielectric slabs are $(b - t) = 1.5\,\text{mm}$. 80 modes are employed in the analysis of the dielectric-filled rectangular waveguides [19]. The computed scattering parameters by the mode-matching method are in good agreement with those calculated by Ansoft's HFSS and it is seen from Fig. 6 that the narrow-banded nature of the longitudinal slot coupling between two parallel rectangular waveguides can be alleviated by inserting dielectric materials.

Waveguide power divider/combiner has wide applications in radar feed systems for its merit of high-power tolerance [20–22]. It is clearly known that a compact-structure can be realized by using dielectric filling. This size reduction may be particularly important for some special applications such as the airborne radar system using slot antenna arrays. Fig. 7 gives an example of 3-port dielectric-filled waveguide power divider. Compared to the conventional waveguide

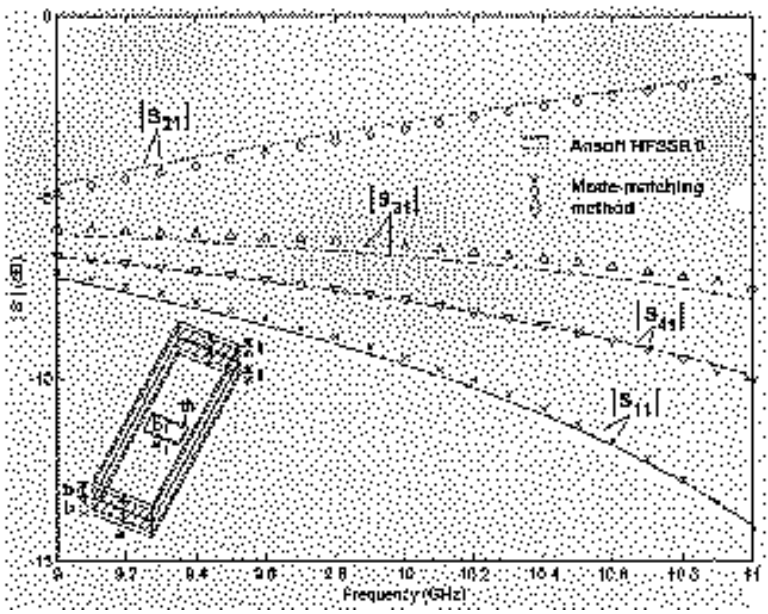

Figure 5. Scattering parameters of a dielectric-filled rectangular-aperture broad-wall coupler ($a = 16.0\,\text{mm}$, $b = 7.5\,\text{mm}$, $a_1 = 9.4\,\text{mm}$, $b_1 = 5.0\,\text{mm}$, $th = 1.0\,\text{mm}$, $t = 2.5\,\text{mm}$, $\varepsilon_{r1} = 1$, $\varepsilon_{r2} = 3.5$).

power dividers/combiners using the standard Magic-T, the dimensions of the device have been greatly reduced and no tuning screws or diaphragms are needed. Dissimilar waveguides are used here due to the structural consideration and an almost even power distribution to port 1 and port 2 is achieved when the input power is from port 3. A satisfactory return loss over the operating frequency band is obtained at the input port ($|\mathbf{S_{33}}|$ in Fig. 7). The relative permittivities for two dielectric slabs used in Fig. 7 are both 3.5 and the thicknesses of two dielectric slabs used in Fig. 7 are $(b_2 - t_1) = 1.5\,\text{mm}$ and $(b_3 - t_2) = 5.0\,\text{mm}$, respectively. The rectangular aperture used for coupling lies at the center of the broad wall in the top T-junction and the center-to-center offset for the aperture in the bottom T-junction is $X_C = 4.5\,\text{mm}$. The bottom T-junction is shortened at a distance $L = 10.0\,\text{mm}$ away from the center of the aperture. In the calculation, 50 modes are considered in the two main waveguides, 20 modes are employed for the rectangular aperture, and 180 modes are used for Region 4 to obtain convergent results. The computed scattering parameters by the mode-matching method are in good agreement with those obtained by Ansoft's HFSS.

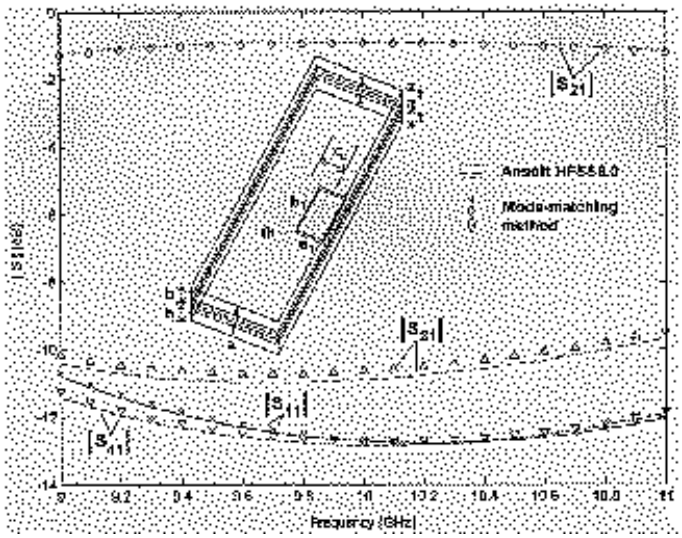

Figure 6. Scattering parameters of a dielectric-filled rectangular-aperture broad-wall coupler ($a = 16.0\,\text{mm}$, $b = 5.0\,\text{mm}$, $a_1 = 5.0\,\text{mm}$, $b_1 = 9.4\,\text{mm}$, $th = 1.0\,\text{mm}$, $t = 3.5\,\text{mm}$, $X_C = 4.5\,\text{mm}$, $\varepsilon_{r1} = 1$, $\varepsilon_{r2} = 3.5$).

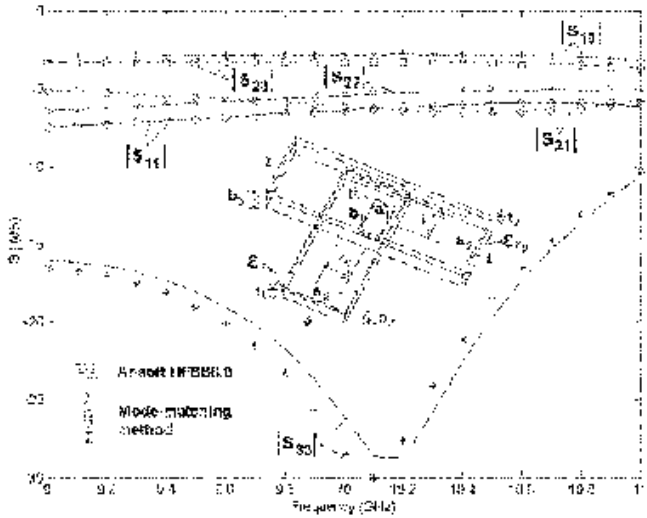

Figure 7. Scattering parameters of a dielectric-filled waveguide power divider ($a_2 = 16.0\,\text{mm}$, $b_2 = 5.0\,\text{mm}$, $b_3 = 7.5\,\text{mm}$, $a_1 = 5.0\,\text{mm}$, $b_1 = 9.4\,\text{mm}$, $th = 1.0\,\text{mm}$, $t_1 = 3.5\,\text{mm}$, $t_2 = 2.5\,\text{mm}$, $X_C = 4.5\,\text{mm}$, $L = 10.0\,\text{mm}$, $\varepsilon_{r1} = 3.5$, $\varepsilon_{r2} = 3.5$).

By narrowing down the aperture, the power enters into the left arm (port 2) and the right arm (port 1) will become closer.

4. CONCLUSION

This paper has described a rigorous full-wave mode-matching analysis of a rectangular waveguide T-junction partially loaded with an H-plane dielectric slab. The longitudinal section electric (LSE) and longitudinal section magnetic (LSM) modes in a dielectric-filled rectangular waveguide are firstly derived and then used in the mode-matching analysis. Numerical results for the scattering parameters of the T-junction are presented and verified by comparing with the available measured data or those obtained by Ansoft's HFSS. Examples for dielectric-filled waveguide couplers and power dividers used in waveguide slot antenna arrays are presented. Excellent agreement has been observed for all the cases considered.

REFERENCES

1. Levy, R., "Directional couplers," *Advances in Microwaves*, L. Young (ed.), Vol. 1, 115–209, Academic Press, New York, 1966.
2. Arndt, F., B. Koch, H. J. Orlok, and N. Schroder, "Field theory design of rectangular waveguide broad-wall metal-insert slot couplers for millimeter-wave applications," *IEEE Trans. Microwave Theory Tech.*, Vol. MTT-33, 95–104, Feb. 1985.
3. Schmiedel, H. and F. Arndt, "Field theory design of rectangular waveguide multiple-slot narrow-wall couplers," *IEEE Trans. Microwave Theory Tech.*, Vol. MTT-34, 791–798, July 1986.
4. Sieverding, T., U. Papziner, and F. Arndt, "Mode-matching CAD of rectangular or circular multiaperture narrow-wall couplers," *IEEE Trans. Microwave Theory Tech.*, Vol. MTT-45, 1034–1040, July 1997.
5. Marcuvitz, N., *Waveguide Handbook*, McGraw-Hill, New York, 1951.
6. Arndt, F., I. Ahrens, U. Papziner, U. Wiechmann, and R. Wilkeit, "Optimized E-plane T-junction series power dividers," *IEEE Trans. Microwave Theory Tech.*, Vol. MTT-35, 1052–1059, Nov. 1987.
7. Sieverding, T. and F. Arndt, "Field theoretic CAD of open or aperture matched T-junction coupled rectangular waveguide structures," *IEEE Trans. Microwave Theory Tech.*, Vol. MTT-40, 353–362, Feb. 1992.

8. Dittloff, J. and F. Arndt, "Rigorous field theory design of millimeter-wave E-plane integrated circuit multiplexers," *IEEE Trans. Microwave Theory Tech.*, Vol. MTT-37, 340–350, Feb. 1989.
9. Sharp, E. D., "An exact calculation for a T-junction of rectangular waveguides having arbitrary cross sections," *IEEE Trans. Microwave Theory Tech.*, Vol. MTT-15, 109–116, Feb. 1967.
10. Liang, X. P., K. A. Zaki, and A. E. Atia, "A rigorous three plane mode-matching technique for characterizing waveguide T-junctions, and its application in multiplexer design," *IEEE Trans. Microwave Theory Tech.*, Vol. MTT-39, 2138–2147, Dec. 1991.
11. Rebollar, J. M., J. Esteban, and J. E. Page, "Fullwave analysis of three and four-port rectangular waveguide junctions," *IEEE Trans. Microwave Theory Tech.*, Vol. MTT-42, No. 2, 256–263, Feb. 1994.
12. Eom, H. J., K. H. Park, J. Y. Kwon, and Y. Yamaguchi, "Fourier-transform analysis for E-plane T-junction in a rectangular waveguide," *Microwave and Optical Tech. Lett.*, Vol. 26, No. 1, 34–37, Wiley, New York, July 2000.
13. Jiang, Z. and Z. Shen, "Mode-matching analysis of large aperture coupling and its applications in designing waveguide directional couplers," submitted for possible publication in *IEEE Trans. Microwave Theory Tech.*, 2002.
14. Datta, A., A. M. Rajeek, A. Chakrabarty, and B. N. Das, "S matrix of a broad wall coupler between dissimilar rectangular waveguides," *IEEE Trans. Microwave Theory Tech.*, Vol. MTT-43, 56–62, Jan. 1995.
15. Collin, R. E., *Field Theory of Guided Waves*, 2nd Ed., IEEE Press, 1991.
16. Angulo, C. M., "Discontinuities in a rectangular waveguide partially filled with dielectric," *IEEE Trans. Microwave Theory Tech.*, Vol. MTT-7, 68–74, Jan. 1957.
17. Uher, J., J. Bornemann, and U. Rosenberg, *Waveguide Components for Antenna Feed System: Theory and CAD*, Artech House, Norwood, MA, 1993.
18. Kuhn, E., "A mode-matching method for solving field problems in waveguide and resonator circuits," *Arch. Elek. Ubertragung*, Vol. 27, 511–518, Dec. 1973.
19. Mittra, R. and S. W. Lee, *Analytical Techniques in the Theory of Guided Waves*, Macmillan, New York, 1971.
20. Hirokawa, J., K. Sakurai, M. Ando, and N. Goto, "An analysis

of a waveguide T-junction with an inductive post," *IEEE Trans. Microwave Theory Tech.*, Vol. MTT-39, No. 3, 563–566, March 1991.

21. Joubert, J. and J. C. Coetzee, "Higher-order mode coupling between H-plane T-junctions and cross-guide slot couplers in feed networks of waveguide slot arrays," *2000 Asia-Pacific Microwave Conference*, 408–411, 2000.
22. Shan, X. and Z. Shen, "A wide-band dielectric-filled transverse-slot antenna array," submitted for possible publication in *IEEE Trans. Antenna and Propagation*, 2002.